

Tiny Sc allows the chains to rattle: Impact of Lu and Y doping on the charge density wave in ScV_6Sn_6

William R. Meier,^{*,†} Richa Pokharel Madhogaria,[†] Shirin Mozaffari,[†] Madalynn Marshall,[‡] David E. Graf,[¶] Michael A. McGuire,[§] Hasitha W. Suriya Arachchige,^{||} Caleb L. Allen,^{||} Jeremy Driver,^{||} Huibo Cao,[‡] and David Mandrus^{*,||}

[†]*Materials Science & Engineering Department, University of Tennessee Knoxville, Knoxville, Tennessee 37996, USA*

[‡]*Neutron Scattering Division, Oak Ridge National Laboratory, Oak Ridge, Tennessee 37831, USA*

[¶]*National High Magnetic Field Laboratory, Tallahassee, FL, 32310, USA*

[§]*Material Science & Technology Division, Oak Ridge National Laboratory, Oak Ridge, Tennessee 37831, USA*

^{||}*Department of Physics & Astronomy, University of Tennessee Knoxville, Knoxville, Tennessee 37996, USA*

[⊥]*Materials Science & Technology Division, Oak Ridge National Laboratory, Oak Ridge, Tennessee 37831, USA*

E-mail: javamochem@gmail.com; dmandrus@utk.edu

Abstract

The kagome metals display an intriguing variety of electronic and magnetic phases arising from the connectivity of atoms on a kagome lattice. A growing number of

these materials with vanadium kagome nets host charge density waves (CDWs) at low temperatures including ScV_6Sn_6 , CsV_3Sb_5 , and V_3Sb_2 . Curiously, only the Sc version of the $R\text{V}_6\text{Sn}_6$ HfFe_6Ge_6 -type materials hosts a CDW ($R = \text{Gd-Lu, Y, Sc}$). In this study we investigate the role of rare earth size in CDW formation in the $R\text{V}_6\text{Sn}_6$ compounds. Magnetization measurements on our single crystals of $(\text{Sc,Lu})\text{V}_6\text{Sn}_6$ and $(\text{Sc,Y})\text{V}_6\text{Sn}_6$ establish that the CDW is suppressed by substitution of Sc by larger Lu or Y. Single crystal x-ray diffraction reveals that compressible Sn-Sn bonds accommodate the larger rare earth atoms within loosely packed R -Sn-Sn chains without significantly expanding the lattice. We propose that Sc provides the extra room in these chains crucial to CDW formation in ScV_6Sn_6 . Our rattling chain model explains why both physical pressure and substitution by larger rare earths hinder CDW formation despite opposite impacts on lattice size. We emphasize the cooperative effect of pressure and rare earth size by demonstrating that pressure further suppresses the CDW in a Lu-doped ScV_6Sn_6 crystal. Our model not only addresses why a CDW only forms in the $R\text{V}_6\text{Sn}_6$ materials with tiny Sc, it also advances to our understanding of why unusual CDWs form in the kagome metals.

Keywords

Charge density wave, intermetallic, stannide, chemical pressure, phase transition, magnetic susceptibility, pressure, x-ray diffraction, ScV_6Sn_6 , RV_6Sn_6 , LuV_6Sn_6 , YV_6Sn_6 , rare earth, phonon

Introduction

A charge density wave (CDW) is an ordered phase of a metallic crystal that appears on cooling. It is characterized by both localization of some conduction electrons and an associated atomic displacement which reduce the translational symmetry of the lattice.^{1,2} CDWs show excellent tune-ability with physical pressure, chemical composition, and disorder.³⁻¹¹

In fact, tuning the CDW transition to zero temperature is a good approach to discover new superconductors.¹²⁻¹⁹

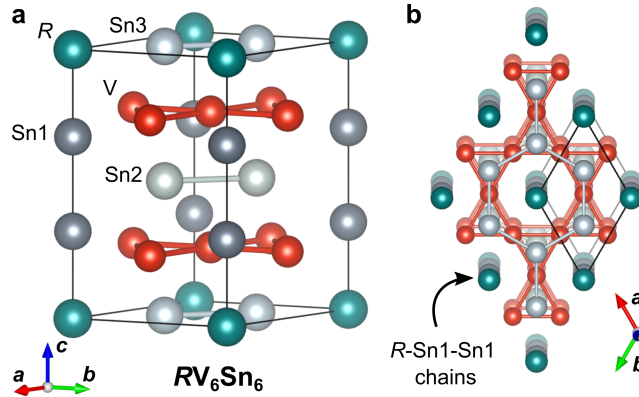


Figure 1: Crystal structure of RV_6Sn_6 . **a** Stacked vanadium-kagome and Sn2/Sn3-honeycomb sheets along c -axis. **b** R -Sn1-Sn1 chains along c fill channels in honeycomb and kagome nets. Generated with VESTA.²⁰

Kagome metals have recently attracted significant interest for their unusual electronic and magnetic properties arising from kagome sheets of transition metals.²¹⁻³⁷ A growing number of these materials display a CDW at low temperature, especially when vanadium forms the kagome net. The AV_3Sb_5 materials ($A = K, Rb, Cs$) host both superconductivity and curious CDW phases.^{23-26,38-50} V_3Sb_2 likely has a CDW transition as well.⁵¹

A CDW has also been identified in the vanadium-kagome metal ScV_6Sn_6 below 92 K.⁵² This is the Sc member of the rare earth RV_6Sn_6 compounds ($R = Sc, Y, \text{ and } Gd-Lu$).⁵³⁻⁵⁵ These adopt the hexagonal $HfFe_6Ge_6$ structure type (Fig. 1a) characterized by V-kagome sheets interleaved between Sn2-honeycomb and Sn3-honeycomb sheets. Rare earth atoms and Sn1 atoms form a chain that occupy channels in the hexagonal holes in the kagome and honeycomb layers as illustrated in Fig. 1b. These chains of atoms play a pivotal role in the CDW mode as they displace along the c -axis in the modulated structure.⁵² Several CDW modes appear to compete in ScV_6Sn_6 ⁵⁶ demonstrated by the strong CDW fluctuations observed above the transition temperature^{57,58} with impacts on the electrical transport properties.²⁷

It is important to note that the CDW in ScV_6Sn_6 has a $\frac{1}{3}\frac{1}{3}\frac{1}{3}$ wave vector^{52,57,58} in con-

trast to that observed in the AV_3Sb_5 materials ($\frac{1}{2}\frac{1}{2}\frac{1}{2}$ or $\frac{1}{2}\frac{1}{2}\frac{1}{4}$).^{23,25,40–43,59,60} Another key difference is that the CDW in AV_3Sb_5 compounds is dominated by vanadium displacements perpendicular to the hexagonal c -axis.²⁵ Numerous investigations of the electronic structure of ScV_6Sn_6 by photoemission measurements tie the CDW order to the Sn bands instead of the prominent vanadium bands.^{58,61–65} There is evidence that the CDW phase has unusual characteristics including anomalous Hall-like responses^{27,66} and claims of time reversal symmetry breaking.⁶⁷

So far, none of the other RV_6Sn_6 appear to host CDW order.^{27,54,55,68–71} What makes the scandium version special? One clue is that the CDW in ScV_6Sn_6 is suppressed by pressure and disappears before 2.4 GPa.⁷² Maybe lattice volume and rare earth size are important.

In this paper, we investigate the impact of rare earth size on CDW formation in the RV_6Sn_6 materials by isovalent substitution of Lu and Y into ScV_6Sn_6 . We synthesize single crystals of $(Sc_{1-x}Lu_x)V_6Sn_6$ and $(Sc_{1-y}Y_y)V_6Sn_6$ and determine the CDW transition temperature with magnetization measurements. We find that the CDW phase is suppressed in both cases without significant impact on the lattice size. Detailed crystallography reveals that larger R atoms are accommodated by extra room between the Sn1-Sn1 atoms along the c -axis (Fig. 1a). We propose that this space in the loose R -Sn1-Sn1 chains is crucial for CDW formation in ScV_6Sn_6 . Our rattling chain model explains why the CDW is suppressed by pressure as well as by doping with larger rare earths despite their opposite impacts on lattice volume. We test our model by confirming that pressure reduces the CDW transition temperature in a sample where instability is already suppressed by Lu-doping. This study answers why only the Sc version of the RV_6Sn_6 kagome metals hosts CDW order; the small Sc atoms provide extra room for R -Sn1-Sn1 chains to rattle and permitting the CDW displacements. In addition this system exhibits an deviation from the usual correspondence between chemical and physical pressure.

Experimental

Crystal growth

Crystals of (Sc,Lu)V₆Sn₆ and (Sc,Y)V₆Sn₆ were grown from a Sn-rich melt following Arachchige et al.⁵² Distilled scandium pieces (Alfa Aesar 99.9%), distilled Lutetium pieces (Alfa Aesar 99.9%), yttrium pieces (Alfa Aesar 99.9%), 3 mm pieces of vanadium slugs (Alfa Aesar 99.8%), and tin shot (Alfa Aesar 99.99+%) were added to 2 or 5 mL alumina Canfield crucible sets.⁷³ An atomic ratio of Sc:Lu:V:Sn or Sc:Y:V:Sn = 1-r:r:6:60 was used for all growths. The crucibles were sealed in silica ampoules filled with about 0.2 atm argon. These were heated in a box furnace to 1150 °C over 12 h and held for 15 h to dissolve as much vanadium as possible. Crystals were grown during a 300 h slow cool to 780 °C. The ampoules were then removed from the furnace, inverted into a centrifuge and spun rapidly to fling the remaining liquid away from the crystals.

These growths yielded hard, light-gray metallic hexagonal crystals on crucible walls and vanadium pieces. Mirror-like basal, prismatic and pyramidal facets are common. The Sc and Lu rich crystals were 0.3–3 mm in size and tend to be blocky with some Sn inclusions. The most Y-rich crystals formed flatter hexagonal plates.

Characterization

Powder x-ray diffraction (XRD) was carried out using a Bruker D2 Phaser with Cu K_α source and Ni filter for phase identification and to determine lattice parameters.

Single crystal x-ray diffraction measurements at room temperature were carried out using a Rigaku XtaLAB PRO diffractometer. Data collection and integration were done using the Rigaku Oxford Diffraction CrysAlis Pro software⁷⁴ and the structural refinement was performed using a SHELXTL package.^{75,76} Refined structures and .cif files of LuV₆Sn₆ and YV₆Sn₆ can be found in the supplemental materials.

Energy disperse spectroscopy (EDS) was performed to estimate the ratios of the rare

earth elements. Crystals were mounted in Crystalbond and polished flat. EDS was carried out in a Zeiss EVO scanning electron microscope at 20 keV.

Magnetization measurements were carried out using a Quantum Design Magnetic Property Measurement System 3 using the Vibrating Sample Magnetometer (VSM) option. Crystals were etched in an aqueous 10 wt% HCl solution for 12-36 h to remove surface Sn then attached to a fused silica paddle with GE varnish. All measurements presented were measured with the field perpendicular to the hexagonal c axis. The fraction of superconducting Sn in each sample was estimated by a 10 Oe zero field cooled measurement through the transition. Estimated beta-Sn fractions ranged from 0.5–7 vol%.

To check for superconductivity, resistance measurements down to 0.12 K were performed using the Adiabatic Demagnetization Refrigerator option in a Quantum Design Physical Property Measurement system using silver paste and platinum wire contacts. These results are presented in the supplemental materials.

Two single crystals of $(\text{Sc}_{1-x}\text{Lu}_x)\text{V}_6\text{Sn}_6$ and one LuV_6Sn_6 crystal were measured concurrently in the same piston cylinder pressure cell. Contacts were made between platinum wire and the samples using Epotek H20E silver epoxy, which was cured at 135°C for 30 minutes. Daphne 7575 was used as a pressure medium⁷⁷ and the value of the pressure was calibrated using the fluorescence of a small ruby chip located near the crystals.⁷⁸ The pressure was recorded at room temperature and again at low temperature, by comparing with the values of fluorescence peaks from a ruby sample at ambient pressure. Resistance measurements were made for each sample using a Lakeshore 372 resistance bridge with 3708 preamp/scanner. The pressure cell was loaded into a Quantum Design Physical Property Measurement System (PPMS) where the temperature was controlled by cooling and warming at a rate of 0.5 K min⁻¹ with about 50 Torr of helium exchange gas in the sample chamber. A calibrated Cernox thermometer was fixed to the outside of the pressure cell next to the copper sample wires to accurately determine the temperature of the measured crystals.

Results

Lattice trends

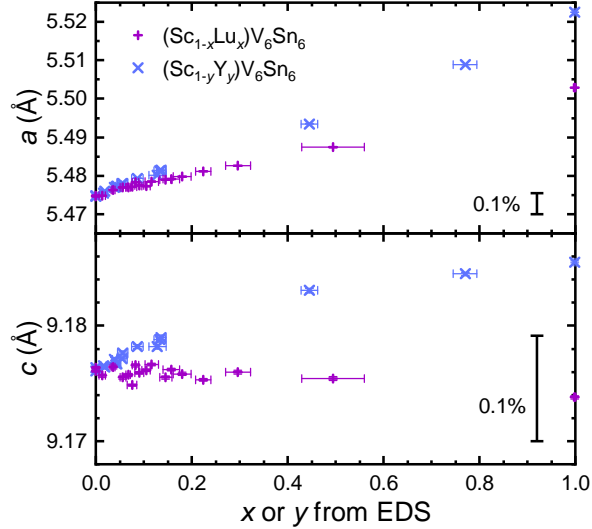


Figure 2: Variation of lattice parameters for $(\text{Sc}_{1-x}\text{Lu}_x)\text{V}_6\text{Sn}_6$ and $(\text{Sc}_{1-y}\text{Y}_y)\text{V}_6\text{Sn}_6$ doping series. Horizontal error bars represent standard deviations of measured x and y by EDS. Vertical error bars are the standard uncertainties from refinements of the lattice parameters. Black vertical bars communicate the size of a 0.1% change in lattice parameters.

Figure 2 presents the evolution the lattice parameters as Y and Lu are doped into ScV_6Sn_6 . a and c vary continuously across both series indicating that a complete solid solution exists. a increases linearly across with a 0.52% and 0.88% expansion to LuV_6Sn_6 and YV_6Sn_6 , respectively. The c parameter increases weakly with Y doping (0.10%) and subtly decreases for the Lu series (-0.02%). Ionic radii provide an imperfect proxy of the size R atoms in $RV_6\text{Sn}_6$. The radii of Sc^{+3} , Lu^{+3} , and Y^{+3} are quoted as 0.87, 0.977, and 1.019 Å at 8-coordinated sites in oxide materials.⁷⁹ Considering the Lu and Y ions are 12% and 17% larger than Sc, it is surprising that the changes in the c lattice parameter are so weak across the substitution series.

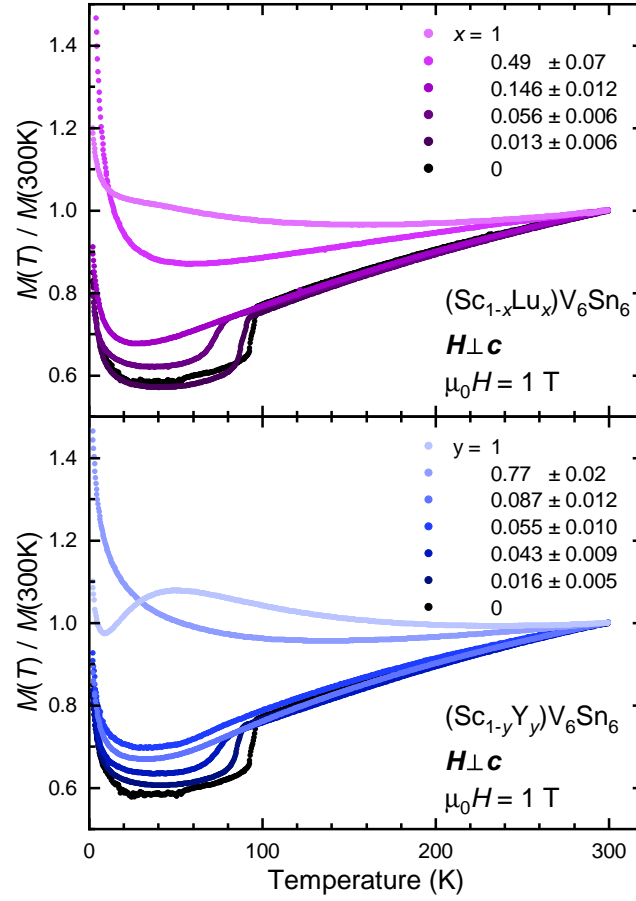


Figure 3: Normalized magnetization vs temperature curves for Lu and Y doped ScV_6Sn_6 . All curves presented were measured on warming after cooling in zero field.

Magnetization

Next we will explore how Lu and Y substitution impacts the CDW in ScV_6Sn_6 . Figure 3 presents the normalized magnetization curves for selected Lu and Y doped samples. The magnitude of the susceptibility at room temperature is comparable for all samples measured, ranging from $7.5\text{--}9.0 \times 10^{-7} \text{ emu g}^{-1} \text{ Oe}^{-1}$ ($6.2\text{--}8.2 \times 10^{-5} \text{ cm}^3 (\text{mol atom})^{-1}$) consistent with Pauli paramagnetism.⁸⁰ The CDW transition in ScV_6Sn_6 manifests as a sharp drop of susceptibility on cooling through the first order transition.⁵² This signature begins at 94 K (black) and shifts to lower temperatures with increasing Lu or Y content. At the same time, the size of drop decreases. The broadening of the transition step is likely due to chemical inhomogeneity observed by EDS.

Phase Diagrams

Figure 4a and b summarizes suppression of the CDW phase with Lu and Y substitution extracted from magnetization. T_{CDW} falls smoothly then discontinuously around a critical doping ($x \approx 0.13$ and $y \approx 0.07$) where we lose the step-like signature. This is not the usual behavior we expect for a quantum critical point where the transition temperature is smoothly reduced to 0 K.⁸¹ Instead, our CDW transition is first order so the phase can disappear more abruptly. No new transitions are observed at higher values of x and y .

It is important to note that less Y is required to destroy the CDW than Lu. This might arise from yttrium's larger size. Figure 4c shows that the trend of T_{CDW} vs average R^{3+} ionic radius has similar behavior for the Lu and Y series. The Lu and Y are also heavier atoms than Sc (174.97, 88.906, and 44.956 g mol⁻¹, respectively). This could be playing a role in suppressing the CDW as proposed by Hu et al.⁶⁵ We suggest that this is less important than size because Lu is heavier than Y and we observe that less Y is needed to destabilize the CDW.

Suppression of a CDW can lead to superconductivity. ADR resistivity measurements revealed no evidence of superconductivity down to at least 150 mK in Lu doped samples

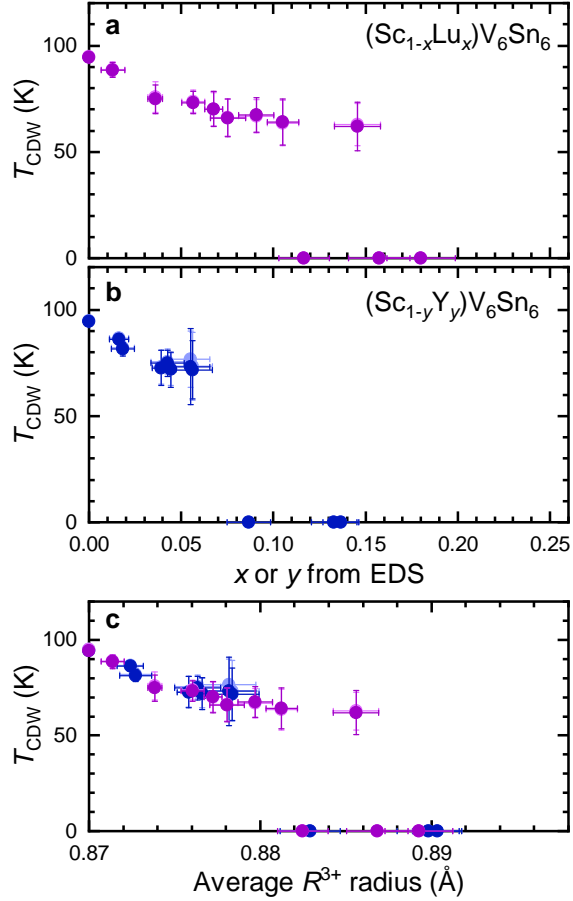


Figure 4: Evolution of T_{CDW} with Lu and Y doping of ScV_6Sn_6 . **a** and **b** Charge density wave temperature (T_{CDW}) vs composition. Horizontal error bars represent standard deviations of Lu/(Sc+Lu) and Y/(Sc+Y) determined by EDS. Vertical bars represent the estimated transition width of the transition based on the drop in the $M(T)$ measurements. Light and dark symbols represent the transition observed on warming and cooling respectively. **c** T_{CDW} vs average ionic radius of R atom.⁷⁹

with $x = 0.157 \pm 0.017$ and 0.180 ± 0.019 as well as Y doped samples with $y = 0.055 \pm 0.010$ and 0.087 ± 0.012 .

Discussion

To simplify our understanding of the evolution of phase transitions we often consider that chemical and mechanical pressure have the same impact on the electronic and lattice subsystems. If lattice volume has a strong impact on the stability of a phase, then we might expect the transition temperature to rise as we expand the lattice with doping (negative chemical pressure) and fall as we compress the lattice mechanically or through doping.

This correspondence between chemical and physical pressure is epitomized by the CDW and superconducting 3-4-13 Remeika phases. Specifically, the $(\text{Sr,Ca})_3\text{Ir}_4\text{Sn}_{13}$ and $(\text{Sr,Ca})_3\text{Rh}_4\text{Sn}_{13}$ substitution series (chemical pressure) exhibit common evolution of the CDW and superconducting critical temperatures with physical pressure.^{10,11}

Our investigation of the CDW evolution in isovalent doped ScV_6Sn_6 reveals behavior that deviates from the universal chemical-physical pressure picture. We observe that the T_{CDW} decrease with negative chemical pressure as we substitute in the larger Lu and Y atom (Fig. 4). Zhang et al. reveal that physical pressure also reduces T_{CDW} .⁷² The observation that CDW in ScV_6Sn_6 is suppressed in both cases suggests a new model is needed to explain this behavior.

Let's begin by looking at how the rare earth atom size actually impacts the lattice. Figure 5 illustrates how the c and a lattice parameters of $RV_6\text{Sn}_6$ compounds depends on R at room temperature. First, observe that most of the the lattice parameters of $RV_6\text{Sn}_6$ compounds (gray points) lie on a linear trend (dashed line) with the smaller, late rare earths with smaller c and a . Sc is the smallest rare earth atom. If only the size matters, we might expect the lattice parameters of ScV_6Sn_6 (dark green star) to lie on the lower left of this trend. This is not the case. It has a smaller a but a comparable c to the Lu compound

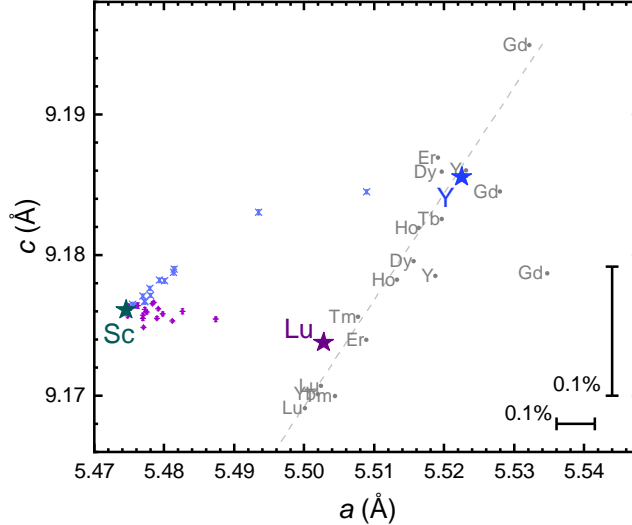


Figure 5: Comparison of room temperature c and a lattice parameters for doped ScV_6Sn_6 and other reported $RV_6\text{Sn}_6$. Gray dots label reported lattice parameters.^{53,55,69,82} Stars represent the lattice parameters of ScV_6Sn_6 , LuV_6Sn_6 , and YV_6Sn_6 determined by powder XRD. The small purple and blue dots are the lattice parameters of the $(\text{Sc,Lu})\text{V}_6\text{Sn}_6$ and $(\text{Sc,Y})\text{V}_6\text{Sn}_6$ doping series, respectively.

(purple star). Obviously, the lattice size is not simply controlled by the size of the rare earth atom. Our doping series emphasize this anomalous lattice evolution in Fig. 5 (small blue and purple symbols) as the lattice parameters interpolate between the end members.

We have established that the c lattice parameter has a nontrivial dependence on the rare earth ion. How are larger R atoms accommodated in the crystal structure if c is only weakly affected? Figure 6 presents the evolution of key bond distances with R ionic radius across the $RV_6\text{Sn}_6$ materials determined by single crystal XRD. To begin, note that larger rare earth atoms produce a larger R -Sn1 bond distance (blue) but the c lattice parameter (black, plotted as $\frac{c}{3}$) increases far more slowly. This requires that the Sn1-Sn1 distance must decrease (red). In other words, larger rare earths compress the Sn1-Sn1 bond with little impact on the unit cell height. Apparently, there is extra room in the R -Sn1-Sn1 chain to accommodate larger atoms.

What is setting the size of c if the R -Sn1-Sn1 chain does not? We propose that the stack of V-kagome and Sn2/Sn3-honeycomb sheets do. Start by considering the $RV_6\text{Sn}_6$ as two subsystems; R -Sn1-Sn1 chains filling tubes in a superstructure of stacked V-kagome and

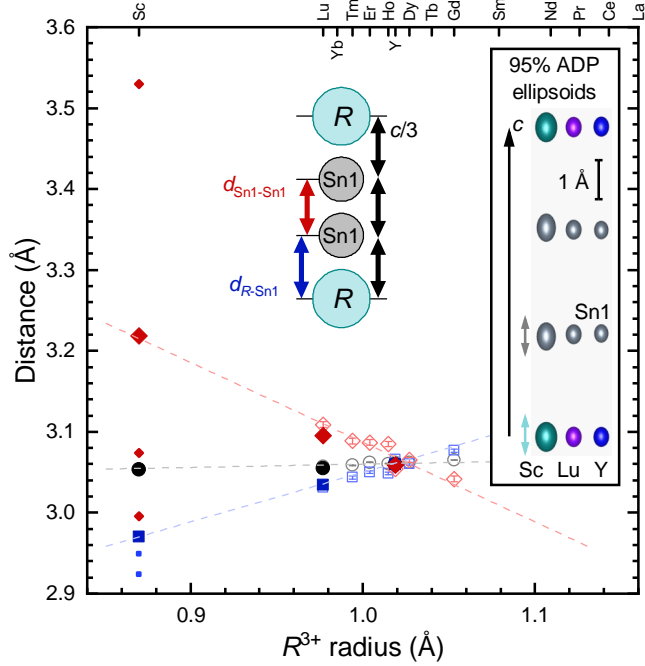


Figure 6: Evolution of bond distances with R^{3+} rare earth ionic radii (coordination number = 8 from Shannon et al.⁷⁹). Large, pale colored marks come from literature.⁵³ Large solid symbols represent distances determined by single crystal x-ray diffraction refinements in this study and Arachchige et al.⁵² Tiny symbols present the Sn1-Sn1 (red) and R -Sn1 (blue) bond lengths in the CDW phase of ScV_6Sn_6 .⁵² The boxed inset depicts the 95% displacement ellipsoids of the R and Sn1 atoms in the refined structures of the Sc, Lu, and Y compounds. The atomic displacement parameters are plotted in supplemental materials.

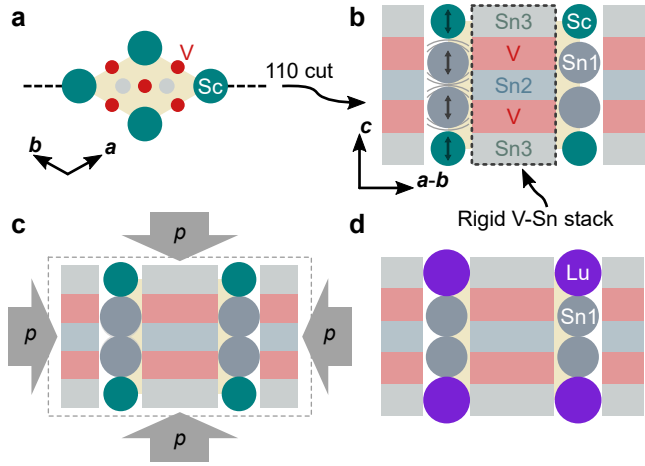


Figure 7: Cartoon of R -Sn1-Sn1 stack. **a** view along $[001]$ of ScV_6Sn_6 structure. **b** (110) cut through the ScV_6Sn_6 structure depicting rigid stack of V-kagome and Sn-honeycomb sheets (colored rectangles) and loosely packed chain of Sc and Sn1 atoms providing room for them to rattle along c . **c** applying pressure compresses the lattice and removes the extra space in the Sc-Sn1-Sn1 chains. **d** replacing Sc with larger Lu compresses the R -Sn1-Sn1 chain and removes the room for the atoms to rattle.

Sn-honeycomb sheets (illustrated in Fig. 1b). Figure 7 depicts a cut along the (110) plane presenting the sections of V and Sn sheets as colored rectangles.

ScV₆Sn₆ and LuV₆Sn₆ have nearly identical c values suggesting that the stacked Sn and V sheets are setting c and small Sc atom leave the channels under-filled (Fig. 7b). This facilitates low-energy rattling displacements of the Sn1. This rattling is evident in the atomic displacement parameters (ADPs) from our single crystal XRD refinements (see supplemental materials). The c -axis displacement parameters, U_{33} , for the R and Sn1 atoms are twice as large in ScV₆Sn₆ than in the Lu or Y compounds. We illustrate this difference in the inset of Fig. 6 by depicting the 95% displacement ellipsoids for the R and Sn1 atoms. The Sc and Sn1 atoms in the first column show taller ellipsoids representing larger position deviations in this direction. This reflects the strong CDW fluctuation observed in ScV₆Sn₆ by inelastic and diffuse x-ray scattering.^{57,58}

These are precisely the displacements that are most prominent in ScV₆Sn₆'s CDW phase. The small symbols in Fig. 6 are the bond lengths in the refined CDW structure of ScV₆Sn₆ from Arachchige et al.⁵² The Sc-Sn1 bonds shrink a little (small blue dots) but, the Sn1-Sn1 bonds vary more dramatically (small red dots). Two Sn1-Sn1 distances shorten by 4.5% and 6.9% while the final third of bonds grow by 9.7%. These Sn1-Sn1 bonds are key feature of CDW and modify the Sn1 p_z orbital states.^{58,65}

We propose that the CDW instability needs the extra space in R -Sn1-Sn1 for the modulations of Sn1-Sn1 distances observed in the CDW. If the column is packed too tightly by larger R atoms or physical pressure, the displacements are penalized.

Next, we will examine how we might expect modifications of ScV₆Sn₆ to impact loose chains of R -Sn1-Sn atoms and, the CDW this facilitates. Applying pressure suppresses T_{CDW} to 0 K by 2.4 GPa.⁷² Pressure compresses the stack of V and Sn sheets (Fig. 7c). This constrains the chain of atoms which shortens the Sn1-Sn1 bonds. The CDW is penalized as the extra room in the chain is removed.

Doping ScV₆Sn₆ with Lu and Y quickly kills the CDW. In this case, introducing larger

atoms fills up the extra room in the R -Sn1-Sn1 chains (Fig. 7d), compressing the Sn1-Sn1 bonds and suppressing the CDW instability. This explains not only why Lu and Y doping suppress the CDW but also why no CDW transition is observed in $RV_6\text{Sn}_6$ with R bigger than Sc.

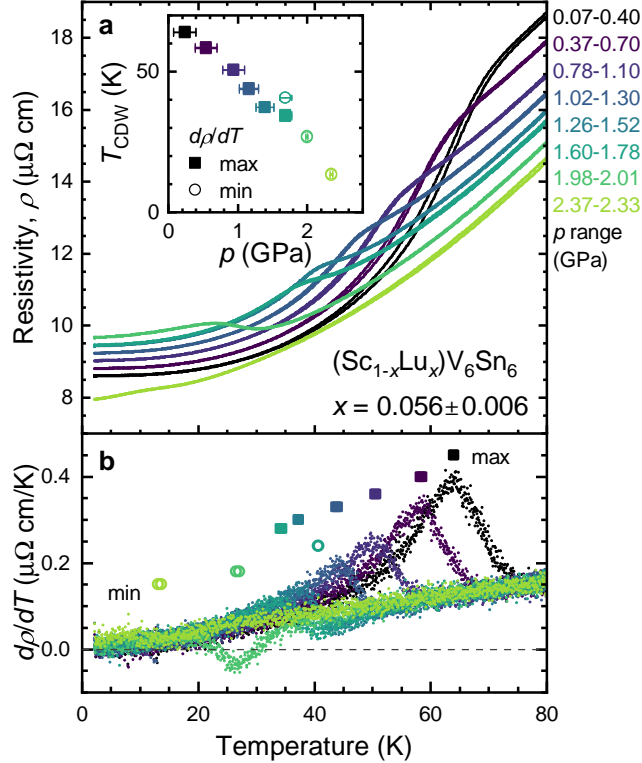


Figure 8: Pressure suppresses the CDW in Lu-doped ScV_6Sn_6 . **a** Resistivity vs temperature plots for $(\text{Sc}_{0.944}\text{Lu}_{0.056})\text{V}_6\text{Sn}_6$ at increasing pressures, p . Resistivity was measured with current perpendicular to the c -axis. The pressures at low and high temp are listed on the right. The inset shows pressure dependence of T_{CDW} . **b** Derivative of $\rho(T)$ highlighting maxima (squares) and minima (circles) used to define T_{CDW} .

This rattling chain mechanism is distinct from the familiar correspondence between chemical and physical pressure. The CDW in ScV_6Sn_6 is suppressed by both lattice compression (physical pressure) and expansion by Lu/Y doping. Our model predicts that pressure and doping by larger rare earth should cooperate to reduce T_{CDW} .

We test this prediction by monitoring the evolution of transition temperature with pressure in a crystal where the CDW is already partly suppressed by Lu-doping. Figure 8 presents the resistance vs temperature of $(\text{Sc}_{0.944}\text{Lu}_{0.056})\text{V}_6\text{Sn}_6$ at a series of pressures. Near atmo-

spheric pressure (black) the CDW transition is observed as a hysteretic drop in resistance on cooling at roughly 64 K. This drop-like feature decreases in temperature as pressure is increased until it changes character to a jump up on cooling for the highest two pressures (observed in pure ScV_6Sn_6 under pressure too⁷²). Applying pressure compresses the V-Sn stack around the already compacted $R\text{-Sn1-Sn1}$ chain in the Lu-doped sample further penalizing the CDW displacements. This observation discredits the possibility that ScV_6Sn_6 has an optimal lattice volume for CDW formation. In that case applying pressure to the Lu-doped sample should re-stabilize the CDW and increase T_{CDW} , but this is not what we observe (see supplemental materials).

Conclusions

In conclusion, we explored how rare earth size impacts CDW formation in the $RV_6\text{Sn}_6$ family. Magnetization measurements on single crystals of $(\text{Sc,Lu})V_6\text{Sn}_6$ and $(\text{Sc,Y})V_6\text{Sn}_6$ revealed that the CDW transition temperature is reduced with increasing Lu and Y content. X-ray diffraction reveals enlightening lattice and bond-length trends. These observations and the evolution of the CDW under pressure motivate us to propose a rattling chain model for CDW formation in the $RV_6\text{Sn}_6$ compounds. We assert that a CDW is only observed in the Sc version of the $RV_6\text{Sn}_6$ compounds because the small Sc atom provides space for Sc and Sn1 atoms to rattle and permit the Sn1-Sn1 bond length modulation observed in the low temperature CDW phase. This model explains why both physical pressure and substitution of Sc by larger rare earth atoms suppresses CDW order. This is a curious variation to the usual corresponding effects of chemical and physical pressure on phase stability. In addition to explaining why ScV_6Sn_6 is special, our observations and model provide an important leap forward in our understanding of CDWs in the intriguing kagome metals.

Acknowledgement

We thank Bryan C. Chakoumakos of Oak Ridge National Laboratory for his helpful discussions with the single crystal x-ray refinements. W.R.M., H.W.S.A., C.L.A., J.D., and D.M. acknowledge support from the Gordon and Betty Moore Foundation’s EPIQS Initiative, Grant GBMF9069. S.M. and R.P.M. acknowledge the support from AFOSR MURI (Novel Light-Matter Interactions in Topologically Non-Trivial Weyl Semimetal Structures and Systems), grant# FA9550-20-1-0322. M.M. and H.B.C. were supported by the U.S. Department of Energy (DOE), Office of Science, Office of Basic Energy Sciences, Early Career Research Program Award KC0402020, under Contract DE-AC05-00OR22725. M.A.M. acknowledges support for adiabatic demagnetization refrigerator resistance measurements from the US Department of Energy, Office of Science, Basic Energy Sciences, Materials Sciences and Engineering Division. A portion of this research used resources at the Spallation Neutron Source, a DOE Office of Science User Facility operated by the Oak Ridge National Laboratory. A portion of this work was performed at the National High Magnetic Field Laboratory, which is supported by National Science Foundation Cooperative Agreement No. DMR-2128556 and the State of Florida.

Supporting Information Available

The following files are available free of charge.

- Supplementary information file including refined structures of LuV_6Sn_6 and YV_6Sn_6 as well resistance under pressure measurements for LuV_6Sn_6 and $(\text{Sc}_{1-x}\text{Lu}_x)\text{V}_6\text{Sn}_6$ with $x = 0.180 \pm 0.019$. Adiabatic demagnetization resistance measurements of doped ScV_6Sn_6 and LuV_6Sn_6 crystals are included as well.
- `LuV6Sn6_20230509.cif` room temperature single crystal refinement of LuV_6Sn_6
- `YV6Sn6_20230519.cif` room temperature single crystal refinement of YV_6Sn_6

References

- (1) Zhu, X.; Guo, J.; Zhang, J.; Plummer, E. W. Misconceptions associated with the origin of charge density waves. *Advances in Physics: X* **2017**, *2*, 622–640.
- (2) Grüner, G. *Density waves in solids*; Perseus Publishing, Cambridge, Mass., 1994.
- (3) Morosan, E.; Zandbergen, H. W.; Dennis, B. S.; Bos, J. W. G.; Onose, Y.; Klimczuk, T.; Ramirez, A. P.; Ong, N. P.; Cava, R. J. Superconductivity in Cu_xTiSe_2 . *Nature Physics* **2006**, *2*, 544–550.
- (4) Joe, Y. I.; Chen, X. M.; Ghaemi, P.; Finkelstein, K. D.; de la Peña, G. A.; Gan, Y.; Lee, J. C. T.; Yuan, S.; Geck, J.; MacDougall, G. J.; Chiang, T. C.; Cooper, S. L.; Fradkin, E.; Abbamonte, P. Emergence of charge density wave domain walls above the superconducting dome in 1T-TiSe₂. *Nature Physics* **2014**, *10*, 421–425.
- (5) Boubeche, M.; Yu, J.; Chushan, L.; Huichao, W.; Zeng, L.; He, Y.; Wang, X.; Su, W.; Wang, M.; Yao, D.-X.; Wang, Z.; Luo, H. Superconductivity and charge density wave in iodine-doped $\text{CuIrCuIr}_2\text{Te}_4$. *Chinese Physics Letters* **2021**, *38*, 037401.
- (6) Kazama, T.; Maeda, M.; Takase, K.; Takano, Y.; Watanabe, T. Electric and magnetic properties of transition-metal carbide Sc_3TC_4 . **2016**, *257*, 34–37.
- (7) Sangeetha, N. S.; Thamizhavel, A.; Tomy, C. V.; Basu, S.; Awasthi, A. M.; Ramakrishnan, S.; Pal, D. Interplay of superconductivity and charge density wave ordering in pseudoternary alloy compounds: $\text{Lu}_2\text{Ir}_3(\text{Si}_{1-x}\text{Ge}_x)_5$, $\text{Lu}_2(\text{Ir}_{1-x}\text{Rh}_x)_3\text{Si}_5$, and $(\text{Lu}_{1-x}\text{Sc}_x)_2\text{Ir}_3\text{Si}_5$. *Physical Review B* **2012**, *86*, 024524.
- (8) Li, Z. et al. Suppressed charge-density-wave, robust ferromagnetism and Lifshitz transition in $\text{Sm}_2\text{Ru}_3\text{Ge}_5$ crystal under high pressure. *Journal of Alloys and Compounds* **2023**, *937*, 168337.

- (9) Veiga, L. S. I.; Mardegan, J. R. L.; v. Zimmermann, M.; Maimone, D. T.; Carneiro, F. B.; Fontes, M. B.; Stremper, J.; Granado, E.; Pagliuso, P. G.; Bittar, E. M. Possible quantum fluctuations in the vicinity of the quantum critical point of $(\text{Sr}, \text{Ca})_3\text{Ir}_4\text{Sn}_{13}$ revealed by high-energy x-ray diffraction. *Physical Review B* **2020**, *101*, 104511.
- (10) Goh, S.; Tompsett, D.; Saines, P.; Chang, H.; Matsumoto, T.; Imai, M.; Yoshimura, K.; Grosche, F. Ambient pressure structural quantum critical point in the phase diagram of $(\text{Ca}_x\text{Sr}_{1-x})_3\text{Rh}_4\text{Sn}_{13}$. *Physical Review Letters* **2015**, *114*, 097002.
- (11) Klintberg, L. E.; Goh, S. K.; Alireza, P. L.; Saines, P. J.; Tompsett, D. A.; Logg, P. W.; Yang, J.; Chen, B.; Yoshimura, K.; Grosche, F. M. Pressure- and composition-induced structural quantum phase transition in the cubic superconductor $(\text{Sr}, \text{Ca})_3\text{Ir}_4\text{Sn}_{13}$. *Physical Review Letters* **2012**, *109*, 237008.
- (12) Sipos, B.; Kusmartseva, A. F.; Akrap, A.; Berger, H.; Forró, L.; Tutiš, E. From Mott state to superconductivity in 1T-TaS₂. *Nature Materials* **2008**, *7*, 960–965.
- (13) Briggs, A.; Monceau, P.; Nunez-Regueiro, M.; Peyrard, J.; Ribault, M.; Richard, J. Charge density wave formation, superconductivity and Fermi surface determination in NbSe₃: A pressure study. *Journal of Physics C: Solid State Physics* **1980**, *13*, 2117–2130.
- (14) Zocco, D. A.; Hamlin, J. J.; Grube, K.; Chu, J.-H.; Kuo, H.-H.; Fisher, I. R.; Maple, M. B. Pressure dependence of the charge-density-wave and superconducting states in GdTe₃, TbTe₃, DyTe₃. *Physical Review B* **2015**, *91*, 205114.
- (15) Zeng, L.; Yan, D.; He, Y.; Boubeche, M.; Huang, Y.; Wang, X.; Luo, H. Effect of Ti substitution on the superconductivity of CuIr₂Te₄ telluride chalcogenide. *Journal of Alloys and Compounds* **2021**, *885*, 160981.

- (16) Aulestia, E. I. P.; Liu, X.; Pang, Y. Y.; So, C. W.; Yu, W. C.; Goh, S. K.; Lai, K. T. Pressure-induced enhancement of the superconducting transition temperature in $\text{La}_2\text{O}_2\text{Bi}_3\text{AgS}_6$. *Journal of Physics: Condensed Matter* **2021**, *34*, 06LT01.
- (17) Eckberg, C.; Campbell, D. J.; Metz, T.; Collini, J.; Hodovanets, H.; Drye, T.; Zavalij, P.; Christensen, M. H.; Fernandes, R. M.; Lee, S.; Abbamonte, P.; Lynn, J. W.; Paglione, J. Sixfold enhancement of superconductivity in a tunable electronic nematic system. *Nature Physics* **2019**, *16*, 346–350.
- (18) Lee, S.; de la Peña, G.; Sun, S. X.-L.; Mitranó, M.; Fang, Y.; Jang, H.; Lee, J.-S.; Eckberg, C.; Campbell, D.; Collini, J.; Paglione, J.; de Groot, F.; Abbamonte, P. Unconventional charge density wave order in the pnictide superconductor $\text{Ba}(\text{Ni}_{1-x}\text{Co}_x)_2\text{As}_2$. *Physical Review Letters* **2019**, *122*, 147601.
- (19) Kudo, K.; Takasuga, M.; Okamoto, Y.; Hiroi, Z.; Nohara, M. Giant phonon softening and enhancement of superconductivity by phosphorus doping of BaNi_2As_2 . *Physical Review Letters* **2012**, *109*, 097002.
- (20) Momma, K.; Izumi, F. VESTA3 for three-dimensional visualization of crystal, volumetric and morphology data. *Journal of Applied Crystallography* **2011**, *44*, 1272–1276.
- (21) Teng, X. et al. Magnetism and charge density wave order in kagome FeGe . *Nature Physics* **2023**,
- (22) Meier, W. R.; Du, M.-H.; Okamoto, S.; Mohanta, N.; May, A. F.; McGuire, M. A.; Bridges, C. A.; Samolyuk, G. D.; Sales, B. C. Flat bands in the CoSn -type compounds. *Physical Review B* **2020**, *102*, 075148.
- (23) Liang, Z.; Hou, X.; Zhang, F.; Ma, W.; Wu, P.; Zhang, Z.; Yu, F.; Ying, J.-J.; Jiang, K.; Shan, L.; Wang, Z.; Chen, X.-H. Three-dimensional charge density wave and surface-dependent vortex-core states in a kagome superconductor CsV_3Sb_5 . *Physical Review X* **2021**, *11*, 031026.

- (24) Kang, M. et al. Twofold van Hove singularity and origin of charge order in topological kagome superconductor CsV_3Sb_5 . *Nature Physics* **2022**, *18*, 301–308.
- (25) Ortiz, B. R.; Teicher, S. M. L.; Kautzsch, L.; Sarte, P. M.; Ratcliff, N.; Harter, J.; Ruff, J. P. C.; Seshadri, R.; Wilson, S. D. Fermi surface mapping and the nature of charge-density-wave order in the kagome superconductor CsV_3Sb_5 . *Physical Review X* **2021**, *11*, 041030.
- (26) Hu, Y.; Wu, X.; Ortiz, B. R.; Ju, S.; Han, X.; Ma, J.; Plumb, N. C.; Radovic, M.; Thomale, R.; Wilson, S. D.; Schnyder, A. P.; Shi, M. Rich nature of van Hove singularities in kagome superconductor CsV_3Sb_5 . *Nature Communications* **2022**, *13*.
- (27) Mozaffari, S. et al. Universal sublinear resistivity in vanadium kagome materials hosting charge density waves. **2023**,
- (28) Colman, R. H.; Sinclair, A.; Wills, A. S. Magnetic and crystallographic studies of Mg-herbertsmithite, $\gamma\text{-Cu}_3\text{Mg}(\text{OH})_6\text{Cl}_2$ - a new $S = 1/2$ kagome magnet and candidate spin liquid. *Chemistry of Materials* **2011**, *23*, 1811–1817.
- (29) Wang, Y.; McCandless, G. T.; Wang, X.; Thanabalasingam, K.; Wu, H.; Bouwmeester, D.; van der Zant, H. S. J.; Ali, M. N.; Chan, J. Y. Electronic properties and phase transition in the kagome metal $\text{Yb}_{0.5}\text{Co}_3\text{Ge}_3$. *Chemistry of Materials* **2022**, *34*, 7337–7343.
- (30) Miiller, W.; Christensen, M.; Khan, A.; Sharma, N.; Macquart, R. B.; Avdeev, M.; McIntyre, G. J.; Piltz, R. O.; Ling, C. D. $\text{YCa}_3(\text{VO})_3(\text{BO}_3)_4$: A kagomé compound based on vanadium(III) with a highly frustrated ground state. *Chemistry of Materials* **2011**, *23*, 1315–1322.
- (31) Gui, X.; Cava, R. J. LaIr_3Ga_2 : A superconductor based on a kagome lattice of Ir. *Chemistry of Materials* **2022**, *34*, 2824–2832.

- (32) Allison, M. C.; Wurmehl, S.; Büchner, B.; Vella, J. L.; Söhnel, T.; Bräuning, S. A.; Klauss, H.-H.; Avdeev, M.; Marlton, F. P.; Schmid, S.; Ling, C. D. FeMn₃Ge₂Sn₇O₁₆: A perfectly isotropic 2-D kagomé lattice that breaks magnetic symmetry with partial spin order. *Chemistry of Materials* **2022**, *34*, 1369–1375.
- (33) Sales, B. C. et al. Chemical control of magnetism in the kagome metal CoSn_{1-x}In_x: Magnetic order from nonmagnetic substitutions. *Chemistry of Materials* **2022**, *34*, 7069–7077.
- (34) Thakur, G. S.; Vir, P.; Guin, S. N.; Shekhar, C.; Weihrich, R.; Sun, Y.; Kumar, N.; Felser, C. Intrinsic anomalous Hall effect in Ni-substituted magnetic weyl semimetal Co₃Sn₂S₂. *Chemistry of Materials* **2020**, *32*, 1612–1617.
- (35) McGuire, M. A.; Zhang, Q.; Miao, H.; Luo, W.; Yoon, M.; Liu, Y.; Yilmaz, T.; Vescovo, E. Antiferromagnetic order and linear magnetoresistance in Fe-substituted shandite Co₃In₂S₂. *Chemistry of Materials* **2021**, *33*, 9741–9749.
- (36) Meschke, V.; Gorai, P.; Stevanović, V.; Toberer, E. S. Search and structural featurization of magnetically frustrated kagome lattices. *Chemistry of Materials* **2021**, *33*, 4373–4381.
- (37) Jovanovic, M.; Schoop, L. M. Simple chemical rules for predicting band structures of kagome materials. *Journal of the American Chemical Society* **2022**, *144*, 10978–10991.
- (38) Ortiz, B. R.; Gomes, L. C.; Morey, J. R.; Winiarski, M.; Bordelon, M.; Mangum, J. S.; Oswald, I. W. H.; Rodriguez-Rivera, J. A.; Neilson, J. R.; Wilson, S. D.; Ertekin, E.; McQueen, T. M.; Toberer, E. S. New kagome prototype materials: discovery of KV₃Sb₅, RbV₃Sb₅, and CsV₃Sb₅. *Physical Review Materials* **2019**, *3*, 094407.
- (39) Ortiz, B. R.; Sarte, P. M.; Kenney, E. M.; Graf, M. J.; Teicher, S. M. L.; Seshadri, R.; Wilson, S. D. Superconductivity in the Z₂ kagome metal KV₃Sb₅. *Physical Review Materials* **2021**, *5*, 034801.

- (40) Ortiz, B. R.; Teicher, S. M. L.; Hu, Y.; Zuo, J. L.; Sarte, P. M.; Schueller, E. C.; Abeykoon, A. M. M.; Krogstad, M. J.; Rosenkranz, S.; Osborn, R.; Seshadri, R.; Balents, L.; He, J.; Wilson, S. D. CsV₃Sb₅: A Z₂ topological kagome metal with a superconducting ground state. *Physical Review Letters* **2020**, *125*, 247002.
- (41) Nie, L. et al. Charge-density-wave-driven electronic nematicity in a kagome superconductor. *Nature* **2022**, *604*, 59–64.
- (42) Wang, Z. et al. Electronic nature of chiral charge order in the kagome superconductor CsV₃Sb₅. *Physical Review B* **2021**, *104*, 075148.
- (43) Li, H. et al. Observation of unconventional charge density wave without acoustic phonon anomaly in kagome superconductors AV₃Sb₅ (A = Rb, Cs). *Physical Review X* **2021**, *11*, 031050.
- (44) Yu, F. H.; Wu, T.; Wang, Z. Y.; Lei, B.; Zhuo, W. Z.; Ying, J. J.; Chen, X. H. Concurrence of anomalous Hall effect and charge density wave in a superconducting topological kagome metal. *Physical Review B* **2021**, *104*, 1041103.
- (45) Jiang, Y.-X. et al. Unconventional chiral charge order in kagome superconductor KV₃Sb₅. *Nature Materials* **2021**, *20*, 1353–1357.
- (46) Yang, S.-Y.; Wang, Y.; Ortiz, B. R.; Liu, D.; Gayles, J.; Derunova, E.; Gonzalez-Hernandez, R.; Šmejkal, L.; Chen, Y.; Parkin, S. S. P.; Wilson, S. D.; Toberer, E. S.; McQueen, T.; Ali, M. N. Giant, unconventional anomalous Hall effect in the metallic frustrated magnet candidate, KV₃Sb₅. *Science Advances* **2020**, *6*.
- (47) Yu, F. H.; Ma, D. H.; Zhuo, W. Z.; Liu, S. Q.; Wen, X. K.; Lei, B.; Ying, J. J.; Chen, X. H. Unusual competition of superconductivity and charge-density-wave state in a compressed topological kagome metal. *Nature Communications* **2021**, *12*.

- (48) Du, F.; Luo, S.; Ortiz, B. R.; Chen, Y.; Duan, W.; Zhang, D.; Lu, X.; Wilson, S. D.; Song, Y.; Yuan, H. Pressure-induced double superconducting domes and charge instability in the kagome metal KV_3Sb_5 . *Physical Review B* **2021**, *103*, 1220504.
- (49) Oey, Y. M.; Ortiz, B. R.; Kaboudvand, F.; Frassinetti, J.; Garcia, E.; Cong, R.; Sanna, S.; Mitrović, V. F.; Seshadri, R.; Wilson, S. D. Fermi level tuning and double-dome superconductivity in the kagome metal $CsV_3Sb_{5-x}Sn_x$. *Physical Review Materials* **2022**, *6*, 1041801.
- (50) Yin, Q.; Tu, Z.; Gong, C.; Fu, Y.; Yan, S.; Lei, H. Superconductivity and normal-state properties of kagome metal RbV_3Sb_5 single crystals. *Chinese Physics Letters* **2021**, *38*, 037403.
- (51) Wang, N. et al. A density-wave-like transition in the polycrystalline V_3Sb_2 sample with bilayer kagome lattice. *Chinese Physics B* **2022**, *31*, 017106.
- (52) Arachchige, H. W. S.; Meier, W. R.; Marshall, M.; Matsuoka, T.; Xue, R.; McGuire, M. A.; Hermann, R. P.; Cao, H.; Mandrus, D. Charge Density Wave in Kagome Lattice Intermetallic ScV_6Sn_6 . *Physical Review Letters* **2022**, *129*, 216402.
- (53) Romaka, L.; Stadnyk, Y.; Romaka, V.; Demchenko, P.; Stadnyshyn, M.; Konyk, M. Peculiarities of component interaction in (Gd, Er)-V-Sn ternary systems at 870 K and crystal structure of RV_6Sn_6 stannides. *Journal of Alloys and Compounds* **2011**, *509*, 8862–8869.
- (54) Zhang, X. X.; Liu, Z. Y.; Cui, Q.; Wang, N. N.; Shi, L. F.; Zhang, H.; Dong, X. L.; Sun, J. P.; Dun, Z. L.; Cheng, J. G. Electronic and magnetic properties of intermetallic kagome magnets RV_6Sn_6 ($R = Tb - Tm$). **2022**,
- (55) Lee, J.; Mun, E. Anisotropic magnetic property of single crystals RV_6Sn_6 ($R = Y, Gd - Tm, Lu$). *Physical Review Materials* **2022**, *6*, 083401.

- (56) Tan, H.; Yan, B. Abundant lattice instability in kagome metal ScV_6Sn_6 . **2023**,
- (57) Cao, S.; Xu, C.; Fukui, H.; Manjo, T.; Shi, M.; Liu, Y.; Cao, C.; Song, Y. Competing charge-density wave instabilities in the kagome metal ScV_6Sn_6 . **2023**,
- (58) Korshunov, A. et al. Softening of a flat phonon mode in the kagome ScV_6Sn_6 . **2023**,
- (59) Neupert, T.; Denner, M. M.; Yin, J.-X.; Thomale, R.; Hasan, M. Z. Charge order and superconductivity in kagome materials. *Nature Physics* **2022**, *18*, 137–143.
- (60) Mu, C.; Yin, Q.; Tu, Z.; Gong, C.; Lei, H.; Li, Z.; Luo, J. *s*-wave superconductivity in kagome metal CsV_3Sb_5 revealed by $^{121/123}\text{Sb}$ NQR and ^{51}V NMR measurements. *Chinese Physics Letters* **2021**, *38*, 077402.
- (61) Cheng, S. et al. Nanoscale visualization and spectral fingerprints of the charge order in ScV_6Sn_6 distinct from other kagome metals. **2023**,
- (62) Kang, S.-H.; Li, H.; Meier, W. R.; Villanova, J. W.; Hus, S.; Jeon, H.; Arachchige, H. W. S.; Lu, Q.; Gai, Z.; Denlinger, J.; Moore, R.; Yoon, M.; Mandrus, D. Emergence of a new band and the Lifshitz transition in kagome metal ScV_6Sn_6 with charge density wave. **2023**,
- (63) Hu, Y. et al. Phonon promoted charge density wave in topological kagome metal ScV_6Sn_6 . **2023**,
- (64) Lee, S.; Won, C.; Kim, J.; Yoo, J.; Park, S.; Denlinger, J.; Jozwiak, C.; Bostwick, A.; Rotenberg, E.; Comin, R.; Kang, M.; Park, J.-H. Nature of charge density wave in kagome metal ScV_6Sn_6 . **2023**,
- (65) Hu, H.; Jiang, Y.; Călugăru, D.; Feng, X.; Subires, D.; Vergniory, M. G.; Felser, C.; Blanco-Canosa, S.; Bernevig, B. A. Kagome materials I: SG 191, ScV_6Sn_6 . Flat phonon soft modes and unconventional CDW formation: Microscopic and effective theory. **2023**,

- (66) Yi, C.; Feng, X.; Yanda, P.; Roychowdhury, S.; Felser, C.; Shekhar, C. Charge density wave induced anomalous Hall effect in kagome ScV_6Sn_6 . **2023**,
- (67) Guguchia, Z. et al. Hidden magnetism uncovered in charge ordered bilayer kagome material ScV_6Sn_6 . **2023**,
- (68) Pokharel, G.; Ortiz, B.; Chamorro, J.; Sarte, P.; Kautzsch, L.; Wu, G.; Ruff, J.; Wilson, S. D. Highly anisotropic magnetism in the vanadium-based kagome metal TbV_6Sn_6 . *Physical Review Materials* **2022**, *6*, 104202.
- (69) Pokharel, G.; Teicher, S. M. L.; Ortiz, B. R.; Sarte, P. M.; Wu, G.; Peng, S.; He, J.; Seshadri, R.; Wilson, S. D. Electronic properties of the topological kagome metals YV_6Sn_6 and GdV_6Sn_6 . *Physical Review B* **2021**, *104*, 235139.
- (70) Ishikawa, H.; Yajima, T.; Kawamura, M.; Mitamura, H.; Kindo, K. GdV_6Sn_6 : A multi-carrier metal with non-magnetic $3d$ -electron kagome bands and $4f$ -electron magnetism. *Journal of the Physical Society of Japan* **2021**, *90*.
- (71) Rosenberg, E.; DeStefano, J. M.; Guo, Y.; Oh, J. S.; Hashimoto, M.; Lu, D.; Birgeneau, R. J.; Lee, Y.; Ke, L.; Yi, M.; Chu, J.-H. Uniaxial ferromagnetism in the kagome metal TbV_6Sn_6 . *Physical Review B* **2022**, *106*, 115139.
- (72) Zhang, X.; Hou, J.; Xia, W.; Xu, Z.; Yang, P.; Wang, A.; Liu, Z.; Shen, J.; Zhang, H.; Dong, X.; Uwatoko, Y.; Sun, J.; Wang, B.; Guo, Y.; Cheng, J. Destabilization of the charge density wave and the absence of superconductivity in ScV_6Sn_6 under high pressures up to 11 GPa. *Materials* **2022**, *15*, 7372.
- (73) Canfield, P. C.; Kong, T.; Kaluarachchi, U. S.; Jo, N. H. Use of frit-disc crucibles for routine and exploratory solution growth of single crystalline samples. *Philos. Mag.* **2016**, *96*, 84–92.
- (74) CrysAlisPRO. Oxford Diffraction/Agilent Technologies UK Ltd, Yarnton, England.

- (75) Sheldrick, G. M. Crystal structure refinement with SHELXL. *Acta Crystallographica Section C Structural Chemistry* **2015**, *71*, 3–8.
- (76) Sheldrick, G. M. SHELXT Integrated space-group and crystal-structure determination. *Acta Crystallographica Section A Foundations and Advances* **2015**, *71*, 3–8.
- (77) Staško, D.; Prchal, J.; Klicpera, M.; Aoki, S.; Murata, K. Pressure media for high pressure experiments, Daphne oil 7000 series. *High Pressure Research* **2020**, *40*, 525–536.
- (78) Piermarini, G. J.; Block, S.; Barnett, J. D.; Forman, R. A. Calibration of the pressure dependence of the R_1 ruby fluorescence line to 195 kbar. *Journal of Applied Physics* **1975**, *46*, 2774–2780.
- (79) Shannon, R. D. Revised effective ionic radii and systematic studies of interatomic distances in halides and chalcogenides. *Acta Cryst.* **1976**, *A32*, 751–767.
- (80) Kittel, C. *Introduction to solid state physics*, eighth ed.; John Wiley & Sons Inc: Hoboken, NJ, 2004.
- (81) Coleman, P.; Schofield, A. J. Quantum criticality. *Nature* **2005**, *433*, 226–229.
- (82) Guo, K.; Ye, J.; Guan, S.; Jia, S. Triangular Kondo lattice in YbV_6Sn_6 and its quantum critical behaviors in magnetic field. **2022**,

TOC Graphic

